Chapter 18

Numerical Calculation for Lightning Response to Grounding Systems Buried in Horizontal Multilayered Earth Model Based on Quasi-Static Complex Image Method

Zhong-Xin Li, Ke-Li Gao, Yu Yin, Cui-Xia Zhang and Dong Ge

Additional information is available at the end of the chapter

http://dx.doi.org/10.5772/57049

1. Introduction

For lightning protection design, an exact evaluation of transients electromagnetic field within a complex grounding system has fundamental importance. In fact, the earth electrodes constitute a fundamental part of the electrical apparatus in both industrial and civil structures. Grounding systems should have a suitable configuration in order to avoid serious hazard to humans, and to preserve electrical insulation in electrical and electronic equipment and installations. Moreover, in electrical power installations, the shape and dimensions of the earth termination system, as a part of a lightning protection system, are more important than the specific value of the earth resistance, in order to disperse the lightning current into the earth without causing dangerous overvoltages.

Pioneering but comprehensive work on this subject was conducted in the first half of the twentieth century, which is summarized by Sunde in the well known reference book [1]. Important pioneering work is described also in [2] and [3]. More recent work is summarized in [4]. Recently, computerized analysis methods have been developed based on different approaches, for example, on circuit theory [5]–[8], transmission line theory [9]–[15], electromagnetic field theory [16]–[23], and hybrid method [24]–[31].

Hybrid method has been developed from conventional nodal analysis, which combines the electrical circuit method and the electromagnetic field method. It has been proved to have combined the strong points of both the two methods. Dawalibi earlier discussed how the hybrid method came out of the electromagnetic field method in [24] and further discussed the hybrid method in [25], however, the hybrid method was based on quasi-static electromagnetic field theory, and only discusses steady grounding problem in the frequency domain. Meliopoulos also discusses the hybrid method based on quasi-static electromagnetic

field theory in [26]; Huang & Kasten developed a new hybrid model to calculate the current distribution in both the grounding system and the metallic support conductors, while considering the voltage drop along the grounding system conductors [27]. However, the model was also based on quasi-static electromagnetic field theory, meanwhile, leakage currents and network currents within the grounding system are separately considered in the calculation, their mutual coupling influence is neglected, and the capacitive coupling effect of the earth is also neglected. Otero, Cidras & Alamo developed a hybrid method to calculate the current distribution in a grounding system [28] within which the mutual inductive and capacitive coupling influence among these current flowing and leaking along the conductor is considered. However, only a uniform half infinite earth model is considered. This hybrid method was combined with the FFT, and so the transient response from the grounding system was obtained. These confines in the frequency domain promoted the development of a novel mathematical model in [29]–[32], which introduced the quasi-static complex image method (QSCIM) for calculating the current distribution in a grounding system buried in both horizontal and vertical multilayered earth models in the frequency domain. However, the hybrid method can be further developed to numerically calculate the transient response from a grounding system buried in multilayered earth model.

Once the multilayered earth model is adopted, the Green's function of a point source will contain an infinite integral for the Bessel function, a complex image method based on Maclaurin's infinite series expansion have been studied in [33] and [34], which has brought up problem about the convergence of the infinite Maclaurin's series. To avoid this convergence problem, QSCIM is introduced to dealt with the infinite integral, which uses finite exponential terms (usually just 3–4 terms) through the Matrix Pencil approach instead of Maclaurin's series to quickly calculate the Green's function.

In this paper, based on previous works [28]–[31], combined with the FFT, a novel and accurate mathematical model is developed for calculating the harmonic wave currents of lightning currents distribution along the grounding system buried in multilayered earth model in the frequency domain, within which not only the conducting effect of the harmonic wave currents leaking into the soil, but also capacitive and inductive effects between different layers of soil have been considered. Both leakage currents and network currents within the grounding system and their mutual coupling are considered in the calculation. The earth is modeled by a multilayered earth model. To accelerate the calculation, QSCIM and closed form of Green's function were introduced, and the mutual inductive and conductive coefficient have analytical formulae so as to avoid numerical integration.

The maximum frequency of applicability of the method is limited by the quasi-static approximation of the electromagnetic fields. For the usual electrodes, it may be applied up to some hundreds of kHz.

2. Frequency domain analysis

The transient problem is first solved by a formulation in the frequency domain. The time-domain response is then obtained by application a suitable Fourier inversion technique. The response to a steady state, time harmonic excitation is computed for a wide range of frequencies starting at zero Hz. From this frequency response, a transfer function is constructed for every frequency considered. The transfer function is dependent only on the geometric and electromagnetic properties of the grounding system and its environment.

http://dx.doi.org/10.5772/57049

if $i(t)$ represents the injected current at a point in the grounding system, and $x(t)$ denotes an observed response, then

$$x(t) = F^{-1}W(j\omega) \cdot F[i(t)] \tag{1}$$

where F and F^{-1} are the Fourier and inverse Fourier transforms, respectively, $W(j\omega)$ is the transfer function, and ω is the angular frequency.

The physical model is based on the following assumptions.

- The earth comprises horizontal multilayered media, and the air media are homogenous and occupy half-spaces with a common horizontal plane boundary between the air and earth.
- The earth and the grounding electrodes exhibit linear and isotropic, arbitrary characteristics.
- The grounding system is assumed to be made of cylindrical metallic conductors with arbitrary orientation. However, they are assumed to be subject to the thin-wire approximation, i.e., the ratio of the length l of the conductor segment to its radius r is $\frac{l}{r} \gg 1$. In practice, a ratio of about 10 is satisfactory.
- Energization occurs by the injection of a current impulse of arbitrary shape produced by an ideal current generator with one terminal connected to the grounding system, and the other to the ground at infinity. The influence of the connecting leads is ignored.

3. Mathematical model of the equivalent circuit of the grounding system in the frequency domain

A set of interconnected cylindrical thin conductors placed in any position or orientation makes up a network to form the grounding system. The grounding network's conductors are assumed to be completely buried in a conductive N_e-layer media (earth) with conductivity σ_e and permittivity $\varepsilon_e = \varepsilon_{r_e} \cdot \varepsilon_0$ (here $e = 1, \cdots\cdots, N_e$). The air is assumed to be a non-conductive medium with permittivity $\varepsilon_0 = \frac{10^{-9}}{36\pi}$ F/m. All media have permeability $\mu = \mu_0 = \frac{10^{-7}}{4\pi}$ H/m.

The proposed methodology is based on the study of all the inductive, capacitive and conductive couplings between the different grounding system conductors. First, the electrode is divided into N_l pieces of segments that can be studied as elemental units, where the discrete grounding system has N_p nodes. A higher segmented rate of the electrode can enhance the model's accuracy but increases its computational time. Therefore, it is necessary to achieve a compromise solution between the two determinants.

The grounding network is energized by injection of single frequency currents at one or more nodes. In general, we consider that a sinusoidal current source of value $\overline{F_j}$ is connected at the jth $(j = 1, 2, \ldots, N_p)$ node. A scalar electric potential (SEP) $\overline{V_j}$ of jth node on the grounding network referring to the infinite remote earth as zero SEP is defined. In the same way, we define an average SEP $\overline{U_k}$ on kth $(k = 1, 2, \ldots, N_l)$ segment. If the segments are short enough, it is possible to consider $\overline{U_k}$ as approximately equal to the average of the kth segment's two terminal nodes SEP. We define a branch current $\overline{I_b^k}$, branch voltage $\overline{U_b^k}$, and leakage current $\overline{I_s^k}$ on the kth $(k = 1, 2, \ldots, N_l)$ segment.

3.1. Mathematical model of the grounding system in the frequency domain

With the above considerations, according to [28]–[31], the electric circuit may be studied using the conventional nodal analysis method [35], resulting in the following equations:

$$[\overline{\mathbf{F}}] = [\overline{\overline{\mathbf{Y}}}] \cdot [\overline{\mathbf{V_n}}] \tag{2}$$

$$[\overline{\overline{\mathbf{Y}}}] = [\overline{\overline{\mathbf{K}}}]^t \cdot [\overline{\overline{\mathbf{Z_s}}}]^{-1} \cdot [\overline{\overline{\mathbf{K}}}] + [\overline{\overline{\mathbf{A}}}] \cdot [\overline{\overline{\mathbf{Z_b}}}]^{-1} \cdot [\overline{\overline{\mathbf{A}}}]^t \tag{3}$$

where $[\overline{\mathbf{F}}]$ is an $N_p \times 1$ vector of external current sources; $[\overline{\overline{\mathbf{Z}_b}}]$ is the $N_l \times N_l$ branch mutual induction matrix of the circuit including resistive and inductive effects, which gives a matrix relationship between branch currents $[\overline{\mathbf{I_b}}]$; $[\overline{\overline{\mathbf{Z_s}}}]$ is an $N_l \times N_l$ mutual impedance matrix, which gives a matrix relationship between the average SEP $[\overline{\mathbf{U}}]$ and leakage currents $[\overline{\mathbf{I_s}}]$ through the rapid Galerkin moment method [38]. Both $[\overline{\overline{\mathbf{A}}}]$ and $[\overline{\overline{\mathbf{K}}}]$ are incidence matrices, which are used to relate branches and nodes. There are rectangular matrices of order $N_l \times N_p$, for whose elements we refer to [28]–[31].

The vector of nodal SEP $[\overline{\mathbf{V_n}}]$ may be obtained by solving 2. The average SEP $[\overline{\mathbf{U}}]$, leakage current $[\overline{\mathbf{I_s}}]$, branch voltage $[\overline{\mathbf{U_l}}]$, and branch current $[\overline{\mathbf{I_b}}]$ can also be calculated [28]–[31].

Once the branch currents and leakage currents are known, the SEP at any point can be calculated by

$$\varphi(\bar{r}_j) = \sum_{i=1}^{N_l} \int_{l_i} G_\varphi(\bar{r}_j, \bar{r}_i) \cdot \frac{I_{s_i}(\bar{r}_i)}{l_i} dl_i \tag{4}$$

where $G_\varphi(\bar{r}_j, \bar{r}_i)$ is the scalar Green's function of a monopole in the multilayered earth model.

The vector magnetic potential (VMP) A at any point can be calculated by

$$\bar{A}(\bar{r}_j) = \sum_{i=1}^{N_l} \int_{l_i} \bar{\bar{G}}_A(\bar{r}_j, \bar{r}_i) \bullet \bar{I}_{b_i}(\bar{r}_i) dt_i. \tag{5}$$

Here, $\bar{\bar{G}}_A(\bar{r}_j, \bar{r}_i)$ is the dyadic Green's function of a dipole in the multilayered earth model, which will be introduced later.

The electrical field intensity (EFI) at any point can be calculated by

$$\bar{E}(\bar{r}_j) = -\sum_{i=1}^{N_l} j\omega \int_{l_i} \bar{\bar{G}}_A(\bar{r}_j, \bar{r}_i) \bullet \bar{I}_{b_i}(\bar{r}_i) dt_i - \sum_{i=1}^{N_l} \nabla \int_{l_i} G_\varphi(\bar{r}_j, \bar{r}_i) \cdot \frac{I_{s_i}(\bar{r}_i)}{l_i} dl_i. \tag{6}$$

http://dx.doi.org/10.5772/57049

The magnetic field intensity (MFI) at any point can be calculated by

$$\bar{B}(\bar{r}_j) = \sum_{i=1}^{N_l} \nabla \times \int_{l_i} \bar{\bar{G}}_A(\bar{r}_j, \bar{r}_i) \bullet \bar{I}_{b_i}(\bar{r}_i) dt_i. \tag{7}$$

The study of the performance of the grounding system in the frequency domain has been reduced to the computation of $[\overline{\overline{\mathbf{Z_s}}}]$ and $[\overline{\overline{\mathbf{Z_b}}}]$ matrices.

3.2. Computation of $[\overline{\overline{\mathbf{Z_b}}}]$ and $[\overline{\overline{\mathbf{Z_s}}}]$ matrices

From [28]–[31], we know that each segment is modeled as a lumped resistance and self-inductance. Mutual inductances or impedances between branch segments' branch currents or leakage currents are also included in the model:

$$[\overline{\overline{\mathbf{X_q}}}]_{N_l \times N_l} = \begin{bmatrix} X_{1,1} & \dots & X_{1,i} & \dots & X_{1,j} & \dots & X_{1,N_l} \\ \vdots & \vdots & \vdots & \vdots & \vdots & \vdots & \vdots \\ X_{i,1} & \dots & X_{i,i} & \dots & X_{i,j} & \dots & X_{i,N_l} \\ \vdots & \dots & \vdots & \dots & \vdots & \vdots & \vdots \\ X_{j,1} & \dots & X_{j,i} & \dots & X_{j,j} & \dots & X_{j,N_l} \\ \vdots & \dots & \vdots & \dots & \vdots & \vdots & \vdots \\ X_{N_l,1} & \dots & X_{N_l,i} & \dots & X_{N_l,j} & \dots & X_{N_l,N_l} \end{bmatrix} \tag{8}$$

1. The case of $[\overline{\overline{\mathbf{X_q}}}] = [\overline{\overline{\mathbf{Z_b}}}]$: $X_{i,i} = R_i + j\omega L_i$, $X_{i,j} = R_{i,j} + j\omega M_{i,j}$.

   The diagonal elements consists of self impedance and self induction, the other elements belong to mutual induction between a pairs of conductor segments. The formula for self impedance and self induction can be found in [28]–[31], here, we give the formula for mutual induction:

$$M_{i,j} = \int_{l_i} \int_{l_j} \bar{\bar{G}}_A(\bar{r}_j, \bar{r}_i) \bullet \bar{I}_{b_i} dt_i \bullet \bar{I}_{b_j i} dt_j \tag{9}$$

   For an infinite homogeneous conductivity medium, one has $\bar{\bar{G}}_A(\bar{r}_j, \bar{r}_i) = \frac{\mu}{4\pi} \frac{1}{R_{ij}} \bar{\bar{I}}^0$, where $\bar{\bar{I}}^0$ is the diagonal unit matrix.

$$M_{i,j} = \frac{\mu}{4\pi} \int_{l_i} \int_{l_j} \frac{1}{R_{ij}} \bar{I}_{b_i} dt_i \bullet \bar{I}_{b_j} dt_j \tag{10}$$

   The above integral can be analytically calculated, this formula can be found in [27].

2. The case of $[\overline{\overline{\mathbf{X_q}}}] = [\overline{\overline{\mathbf{Z_s}}}]$: $X_{i,j} = Z_{i,j}$.

   $Z_{i,j}$ is the mutual impedance coefficient between a pair of conductor segments in the grounding system. The matrix above includes the conductive and capacitive effects of the earth, and its elements are the mutual impedance coefficients $Z_{i,j}$.

$$Z_{i,j} = \int_{l_i}\int_{l_j} G_\varphi(\bar{r}_j, \bar{r}_i)\ \frac{dt_i}{l_i}\frac{dt_j}{l_j} \tag{11}$$

   For an infinite homogeneous conductivity medium, one has $G_\varphi(\bar{r}_j, \bar{r}_i) = \frac{1}{4\pi\bar{\sigma}_1}\frac{1}{R_{ij}}$, so

$$Z_{i,j} = \frac{1}{4\pi\bar{\sigma}_1 l_j l_j}\int_{l_i}\int_{l_j}\frac{1}{R_{ij}}dt_i dt_j \tag{12}$$

   where $\bar{\sigma}_1 = \sigma_1 + j\omega\varepsilon_1$. Eq. (12) can be solved analytically [36].

Note the medium surrounding the point current source here was considered as homogeneous and infinite. However, in any practical case, the earth is represented via a multilayered earth model. The QSCIM can be used to dealt with the multilayered earth model, this will be discussed next.

4. The closed form of the Green's function of a point source in a horizontal multilayered earth model and the QSCIM

The closed form of the Green's function of a scalar monopole and vector dipole buried in horizontal multilayered earth model will be respectively introduced.

4.1. The closed form of the Green's function of a scalar point source in a horizontal multilayered earth model and the QSCIM

The main task of simulation grounding system is calculating the element Z_{jk} of matrix $[\overline{\overline{\mathbf{Z_s}}}]$ in Eq. (11). When the earth model is considered as horizontal multilayered conductivity media, influences from the interface will be considered, which will lead to infinite integral about Bessel function associated with Green's function of a scalar monopole. However, the element Z_{jk} of matrix $[\overline{\overline{\mathbf{Z_s}}}]$, which includes the Green's function, can be fast calculated by using the QSCIM.

To perform the calculation, the corresponding Green's function of a scalar monopole must be defined first. The Green's function can be regarded as the SEP of one point located at any place produced by a scalar monopole with unit current δ in a horizontal multilayered conducting medium. For low frequency (50 or 60 Hz and higher harmonic wave) and limited size of the substation, the propagating effect of electromagnetic wave can be neglected, so

http://dx.doi.org/10.5772/57049

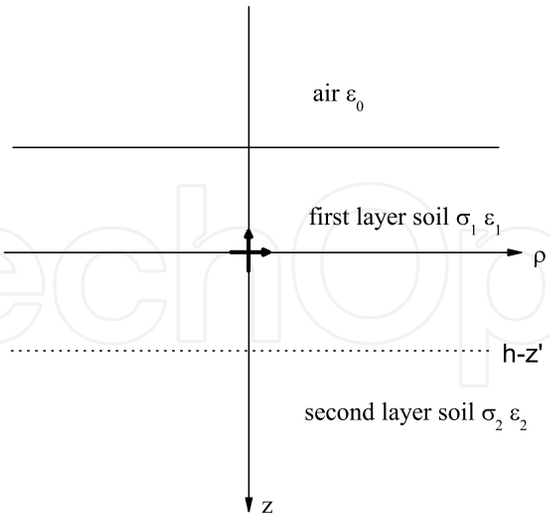

Figure 1. The earth model

the electromagnetic field here can be regarded as quasi-static field, so the SEP φ satisfies the Poisson equation as:

$$\nabla^2 \varphi_j = -\frac{\delta(r, r')\delta(ij)}{\overline{\sigma_i}} \tag{13}$$

where $i, j = 1, \ldots, N_s$, and $\delta(r, r')$ is the Dirac delta function. $\delta(ij)$ is Kronecker's symbol, $\overline{\sigma_i} = \sigma_i + j\omega\varepsilon_i$ is the complex conductivity of the ith layer medium. Supposing the monopole is located at origin of the coordinate system, seen from Fig. 1.

If the monopole lies in infinite homogenous medium, its expression of Green's function in the spherical coordinate system is.

$$\varphi = G(\bar{r}, \bar{r'}) = \frac{1}{4\pi \cdot \overline{\sigma} \cdot R} \tag{14}$$

where $R = |\bar{r} - \bar{r'}|$ is the distance between the source point and field point. While its expression in the cylindrical coordinates system (ρ, z) is as follows:

$$\varphi = G(\rho, z) = \frac{1}{4\pi \cdot \overline{\sigma}} \int_0^\infty e^{-\lambda|z|} J_0(\lambda\rho) d\lambda \tag{15}$$

where $J_0(\lambda\rho)$ is the Bessel function of the first kind of order zero.

For horizontal multilayered earth model, for examples, two-layer earth model, in the cylindrical coordinate system, the general form of Green's functions can be expressed by [1]:

$$\varphi_{10} = G_{10}(\rho, z) = \frac{1}{4\pi \cdot \overline{\sigma}_1} \int_0^\infty \left[A_{10}(\lambda) e^{-\lambda \cdot z} + B_{10}(\lambda) e^{+\lambda \cdot z} \right] J_0(\lambda\rho) d\lambda \tag{16}$$

$$\varphi_{11} = G_{11}(\rho, z) = \frac{1}{4\pi \cdot \overline{\sigma}_1} \int_0^\infty \left[e^{-\lambda|z|} + A_{11}(\lambda) e^{-\lambda z} + B_{11}(\lambda) e^{+\lambda z} \right] J_0(\lambda\rho) d\lambda \tag{17}$$

$$\varphi_{12} = G_{12}(\rho, z) = \frac{1}{4\pi \cdot \overline{\sigma}_1} \int_0^\infty \left[A_{12}(\lambda) e^{-\lambda \cdot z} + B_{12}(\lambda) e^{+\lambda \cdot z} \right] J_0(\lambda\rho) d\lambda \tag{18}$$

where G_{10}, G_{11} and G_{12} express the Green's function for the field point in the air, the top layer and bottom layer, respectively.

The six constants $A_{10} \sim B_{12}$ can be determined by employing the interface and infinite conditions of the SEP ($\varphi_{10} = \varphi_{11}$, $\sigma_0 \frac{\partial \varphi_{10}}{\partial z} = \sigma_1 \frac{\partial \varphi_{11}}{\partial z}$, $\varphi_{11} = \varphi_{12}$, $\sigma_1 \frac{\partial \varphi_{11}}{\partial z} = \sigma_2 \frac{\partial \varphi_{12}}{\partial z}$, $\varphi_{10}|_{z \mapsto -\infty} = 0$ and $\varphi_{12}|_{z \mapsto +\infty} = 0$).

Consequently, the expression of G_{11} can be given as follows:

$$G_{11}(\rho, z) = \frac{1}{4\pi\overline{\sigma}_1} \int_0^\infty [e^{-k_\rho|z|} - k_{01} e^{-k_\rho(2z'+z)} + f(k_\rho)(k_{01}^2 k_{12} e^{-k_\rho(2h+2z'+z)}$$

$$- k_{01} k_{12} e^{-k_\rho(2h+z)} + k_{12} e^{-k_\rho(2h-2z'-z)} - k_{01} k_{12} e^{-k_\rho(2h-z)})] J_0(k_\rho\rho) dk_\rho \tag{19}$$

where $f(\lambda) = \frac{k_{12}}{(1+k_{01}k_{12}e^{-2\lambda \cdot h})}$,$k_{01} = \frac{(\overline{\sigma}_0 - \overline{\sigma}_1)}{(\overline{\sigma}_0 + \overline{\sigma}_1)}$, $k_{12} = \frac{(\overline{\sigma}_1 - \overline{\sigma}_2)}{(\overline{\sigma}_1 + \overline{\sigma}_2)}$, h is the thickness of the top layer, $\overline{\sigma}_0$,$\overline{\sigma}_1$ and $\overline{\sigma}_2$ are the complex conductivity of air and two layers, respectively.

Now this $f(\lambda)$ can be developed into an exponential series with finite terms by MP method [37] instead of Maclaurin's series to avoid verbose calculation [38]:

$$f(\lambda) = \sum_{n=1}^{N} \alpha_n \cdot e^{\beta_n \lambda} \tag{20}$$

http://dx.doi.org/10.5772/57049

where α_n and β_n are constants to be determined by choosing sample points of function $f(\lambda)$.

Considering the Laplace transform of Bessel function of the first kind of order v $J_v(\lambda\rho)$, we have [39]

$$\int_0^\infty e^{-c\lambda} J_v(\lambda\rho)d\lambda = \left[\frac{\rho}{c+\sqrt{\rho^2+c^2}}\right]^v \frac{1}{(c^2+\rho^2)^{\frac{1}{2}}} \tag{21}$$

where $Re(v) > -1$ and $Re(c) > 0$.

Set $v = 0$, so we have Lipschitz integration:

$$\int_0^\infty e^{-c\lambda} J_0(\lambda\rho)d\lambda = \frac{1}{(c^2+\rho^2)^{\frac{1}{2}}} \tag{22}$$

By employing Eq. (20) and Lipschitz integration, the closed form of the Green's function (Eq. (19)) can be given as following:

$$G_{11}(\bar{r},\bar{r'}) = \frac{1}{4\pi\overline{\sigma}_1}[\frac{1}{R_0} - \frac{k_{01}}{R_0'} + \sum_{n=1}^{N}\alpha_n(\frac{k_{01}^2 k_{12}}{R_{n1}} - \frac{k_{01}k_{12}}{R_{n2}} + \frac{k_{12}}{R_{n3}} - \frac{k_{01}k_{12}}{R_{n4}})] \tag{23}$$

where the origin of the coordinate system shown in Fig. 1 has been moved to the surface of the earth, the source point is at $(0, z')$ and the field point is at (ρ, z), so $R_0 = [\rho^2 + (z-z')^2]^{\frac{1}{2}}$, in the same way, we have $R_0^{'} = [\rho^2 + (z+z')^2]^{\frac{1}{2}}$, $R_{n1} = [\rho^2 + (z+z'-z_n)^2]^{\frac{1}{2}}$, $R_{n2} = [\rho^2 + (z - z'-z_n)^2]^{\frac{1}{2}}$, $R_{n3} = [\rho^2 + (z+z'+z_n)^2]^{\frac{1}{2}}$, $R_{n4} = [\rho^2 + (z-z'+z_n)^2]^{\frac{1}{2}}$, in which $z_n = 2h - \beta_n$.

It can be seen that each term except $\frac{1}{R_0}$ of Eq. (23) can be regarded as a image scalar monopole source, whose location is indicated by $R_{ni,i=1\backsim4}$ and amplitude is α_n, which can be seen in Fig. 1. However, in Eq. (23) α_n and R_{ni} are usually complex numbers, so that this approach is named as the QSCIM.

G_{10} and G_{12} can be similarly gotten.

The procedure for the closed form of the Green's function of a scalar monopole in arbitrary horizontal multilayered earth model is first to derive the specific solution of the Green's function in each layer based on the general expressions (for example, the general expressions of a scalar monopole in three layers media is given in Eq. (15), Eq. (16) and Eq. (17)), and the interface and infinite conditions of SEP of the monopole is used to decide the unknown constants. Then, by employing the MP method exponential series development and the Lipschitz integration, the final expression of the Green's functions can be obtained.

Once the closed form of Green's function of a scalar monopole in the horizontal multilayered earth model has been gotten, the mutual impedance coefficient Eq. (11) can be fast analytical calculated, which is just same as the Eq. (12).

4.2. The closed form of the Green's function of a vector point source in a horizontal multilayered earth model and the QSCIM

The another important task of simulation grounding system is calculating the element M_{jk} of matrix $[\overline{\overline{\mathbf{Z_b}}}]$ in Eq. (9). When the earth model is considered as horizontal multilayered conductivity media, and influences from the interfaces on mutual induction between two conductors should be considered, which also lead to infinite integral about Bessel function in the Green's function of a vector dipole, the element M_{jk} of matrix $[\overline{\overline{\mathbf{Z_b}}}]$ includes the Green's function, which can also be fast calculated by using the QSCIM.

Like Green's function of the scalar monopole, to perform the calculation of a vector dipole in horizontal multilayered earth model, its corresponding Green's function should also be defined first. The Green's function can be regarded as the VMP A of a point at any place produced by a vector dipole with unit current δ within a horizontal multilayered medium, whose electromagnetic field can also be regarded as quasi-static field, so the VMP A also satisfies the Poisson equation as:

$$\nabla^2 A_j = -\mu\bar{\delta}(r, r')\delta(ij) \tag{24}$$

where $i, j = 1, \ldots, N_s; \mu$ is the permeability of the earth medium. Supposing the dipole is located at origin of the coordinate system, seen from Fig. 1

If the vector dipole is lying in homogenous infinite medium, its expression of Green's function in the spherical coordinate system is.

$$A = G_A(r, r') = \frac{\mu}{4\pi \cdot R} \tag{25}$$

And its expression in the cylindrical coordinates system (ρ, z) is as follows:

$$A = G_A(\rho, z) = \frac{\mu}{4\pi} \int_0^\infty e^{-\lambda|z|} J_0(\lambda\rho) d\lambda \tag{26}$$

Not like scalar monopole source, for horizontal multilayered earth model, vector dipole source must be considered into two cases, which are vertical and horizontal dipoles, respectively. This is because any placed dipole in horizontal multilayered earth model can be decomposed into horizontal and vertical components. For vertical dipole case, its Green's function can be defined as $G^z_{A_z}$; For horizontal dipole case, it own two components, which are horizontal x or y component and vertical z component, so its Green's function can be defined as $G^x_{A_x}$ and $G^z_{A_x}$, respectively.

We also take the two-layer earth model as an example, the dipole lies in the earth model. In the cylindrical coordinate system, the general form of Green's functions for the vertical dipole $G^z_{A_z}$ or horizontal dipole $G^x_{A_x}$ can be expressed by [1]:

http://dx.doi.org/10.5772/57049

$$A_{p10}^{p} = G_{A_{p10}}^{p}(\rho, z) = \frac{\mu}{4\pi}\int_0^{\infty}\left[A_{10}(\lambda)e^{-\lambda\cdot z} + B_{10}(\lambda)e^{+\lambda\cdot z}\right]J_0(\lambda\rho)d\lambda \tag{27}$$

$$A_{p11}^{p} = G_{A_{p11}}^{p}(\rho, z) = \frac{\mu}{4\pi}\int_0^{\infty}\left[e^{-\lambda\cdot|z|} + A_{11}(\lambda)e^{-\lambda\cdot z} + B_{11}(\lambda)e^{+\lambda\cdot z}\right]J_0(\lambda\rho)d\lambda \tag{28}$$

$$A_{p12}^{p} = G_{A_{p12}}^{p}(\rho, z) = \frac{\mu}{4\pi}\int_0^{\infty}\left[A_{12}(\lambda)e^{-\lambda\cdot z} + B_{12}(\lambda)e^{+\lambda\cdot z}\right]J_0(\lambda\rho)d\lambda \tag{29}$$

where $G_{A_{p10}}^{p}$, $G_{A_{p11}}^{p}$ and $G_{A_{p12}}^{p}$ express the Green's function of the dipole for the field point in the air, the top layer and bottom layer, respectively; for vertical dipole case, $p = z$, for horizontal dipole case, $p = x$.

Just like the deduced procedure for Green's function of a scalar monopole, the six constants $A_{10} \sim B_{12}$ can also be decided by employing the interface and infinite conditions of the dipole's VMP. For vertical dipole, there is a $f(\lambda)$, which can also be developed into an exponential series with finite terms by the MP method. Last by applying the Lipschitz integration, the final expression of $G_{A_{p11}}^{p}$ can be given as follows.

$$G_{A_{z11}}^{z}(\bar{r}, \bar{r'}) = \frac{\mu}{4\pi}\left[\frac{1}{R_0} + \frac{k_{01}}{R_0'} - \sum_{n=1}^{N}\alpha_n\left(\frac{k_{01}^2 k_{12}}{R_{n1}} + \frac{k_{01}k_{12}}{R_{n2}} - \frac{k_{12}}{R_{n3}} + \frac{k_{01}k_{12}}{R_{n4}}\right)\right] \tag{30}$$

$$G_{A_{x11}}^{x}(\rho, z) = \frac{\mu}{4\pi\ R_0} \tag{31}$$

where the origin of the coordinate system shown in Fig. 1 has been moved to the surface of the earth. R_0, R_0', $R_{ni,i=1\backsim4}$ are just same as Eq. (23).

For horizontal dipole, there is a Green's function for z component $G_{A_{x11}}^{z}$ left, in the cylindrical coordinate system, the general form of the Green's function for z component in the two-layer earth model can be expressed by [1]:

$$A_{x10}^{z} = G_{A_{x10}}^{z}(\rho, z) = \frac{\mu}{4\pi}\frac{\partial}{\partial x}\int_0^{\infty}\left[A_{10}(\lambda)e^{-\lambda\cdot z} + B_{10}(\lambda)e^{+\lambda\cdot z}\right]J_0(\lambda\rho)\frac{d\lambda}{\lambda} \tag{32}$$

$$A_{x11}^{z} = G_{A_{x11}}^{z}(\rho, z) = \frac{\mu}{4\pi}\frac{\partial}{\partial x}\int_0^{\infty}\left[A_{11}(\lambda)e^{-\lambda z} + B_{11}(\lambda)e^{+\lambda z}\right]J_0(\lambda\rho)\frac{d\lambda}{\lambda} \tag{33}$$

$$A_{x12}^{z} = G_{A_{x12}}^{z}(\rho, z) = \frac{\mu}{4\pi}\frac{\partial}{\partial x}\int_0^{\infty}\left[A_{12}(\lambda)e^{-\lambda\cdot z} + B_{12}(\lambda)e^{+\lambda\cdot z}\right]J_0(\lambda\rho)\frac{d\lambda}{\lambda} \tag{34}$$

Also like the deduced procedure for Green's function of a scalar monopole, the six constants $A_{10} \sim B_{12}$ can be decided by employing the interface and infinite conditions of the horizontal dipole's VMP. The $f(\lambda)$ in the Green's function can also be developed into an exponential series with finite terms by the MP method. Last by applying the Lipschitz integration's varied form ($\int_0^{\infty} e^{-c\lambda}J_0(\lambda\rho)\frac{d\lambda}{\lambda} = \ln(c+\sqrt{c^2+\rho^2})$), the final expression of $G_{A_{x11}}^{z}$ can be given as follows.

$$G_{A_{x11}}^{z}(\rho, z) = \frac{\mu}{4\pi}\frac{\partial}{\partial x}[k_{01}\ln(z_0^{'} + R_0^{'}) - \sum_{n=1}^{N}\alpha_n(k_{01}^2 k_{12}\ln(z_{n1} + R_{n1})$$

$$+ k_{01}k_{12}\ln(z_{n2} + R_{n2}) - k_{12}\ln(z_{n3} + R_{n3}) + k_{01}k_{12}\ln(z_{n4} + R_{n4}))] \tag{35}$$

where the origin of the coordinate system shown in Fig. 1 has been moved to the surface of the earth. The R_0' and $R_{ni,i=1\backsim4}$ are same as Eq. (23). Other parameters are $z_0^{'} = z + z'$, $z_{n(1-4)} = (sign_a \cdot z + sign_b \cdot z') + z_n$, in which $sign_a = 1$ for z_{n1} and z_{n3}, $sign_b = 1$ for z_{n3} and z_{n4}, $sign_a = sign_b = -1$ for others.

It can also be seen that each term except $\frac{1}{R_0}$ of Eqs. (30) and (35) can be regarded as a image vector dipole source, whose location is indicated by $R_{ni,i=1\backsim4}$ and amplitude is α_n, which can be seen in Fig. 1. However, in Eqs. (30) and (35), α_n and R_{ni} are usually complex numbers, so that this approach is also named as the QSCIM.

The other Green's function for the dipole $G_{A_{z10}}^{z}$, $G_{A_{z12}}^{z}$, $G_{A_{x10}}^{x}$, $G_{A_{x12}}^{x}$, $G_{A_{x10}}^{z}$ and $G_{A_{x12}}^{z}$ can be given in the similarly way.

Like closed form of Green's function of a scalar monopole, the procedure for the closed form of the Green's function of a vector dipole in arbitrary horizontal multilayered earth model is also first to derive the specific solution of the Green's function in each layer based on the general expressions (for example, the general expressions of Green's function for a vertical dipole or x component of horizontal dipole in three horizontal layers medium are given in Eq. (27), Eq. (28) and Eq. (29); for z component of horizontal dipole, are given in Eq. (32), Eq. (33) and Eq. (34)), and the interface and infinite conditions of VMP of the dipole are also used to decide unknown constants. Then, for z component of horizontal dipole and vertical dipole, by employing the MP method exponential series can be developed. Last by utilizing the Lipschitz integration and its varied form, the final expression of the Green's function of the dipole can be achieved.

Once the closed form of Green's function of a vector dipole in horizontal multilayered earth model has been given, the mutual impedance coefficient Eq. (9) can also be fast analytical calculated just like Eq. (10).

http://dx.doi.org/10.5772/57049

5. Time-domain solutions

Once the transfer functions $W(j\omega)$ have been determined for each calculated quantity, for example the electric field or current at specified points, the time-domain solutions can be obtained by direct application of (1). The calculation of the inverse Fourier transform is carried out by an FFT algorithm which is well-suited for the evaluation of time-domain responses.

The transient impedance, an essential parameter in grounding system design, is defined as a ratio of time varying voltage and current at injection point [19]:

$$Z(t) = \frac{v(t)}{i(t)} \tag{36}$$

where $i(t)$ represents the injected current at a grounding grid. This injected current represents the lightning channel current usually expressed by the double exponential function $i(t) = I_m(e^{-\alpha t} - e^{-\beta t})$, $t \geq 0$, where pulse rise time is determined by constants α and β, while I_m denotes the amplitude of the current waveform. The Fourier transform of the excitation function is defined by integral [40]:

$$I(f) = \int_{-\infty}^{\infty} i(t) e^{j2\pi f t} dt \tag{37}$$

Integral (37) can be evaluated analytically

$$I(f) = I_m\left(\frac{1}{\alpha + j2\pi f} - \frac{1}{\beta + j2\pi f}\right) \tag{38}$$

The frequency components up to few MHz are meaningfully present in the lightning current Fourier spectrum with strong decreasing importance from very low to highest frequencies. Multiplying the excitation function $I(f)$ with the input impedance spectrum $Z_{in}(f)$ provides the frequency response of the grounding system:

$$U(f) = I(f) Z_{in}(f) \tag{39}$$

Applying the IFFT, a time domain voltage counterpart is obtained. IFFT of the function $U(f)$ is defined by the integral [40]:

$$U(t) = \int_{-\infty}^{\infty} U(f) e^{j2\pi f t} d\omega \tag{40}$$

As the frequency response $U(f)$ is represented by a discrete set of values the integral (41) cannot be evaluated analytically and the discrete Fourier transform, in this case the IFFT algorithm, is used, i.e.,

$$U(t) = IFFT(U(f)) \tag{41}$$

Implementation of this algorithm inevitably causes an error due to discretization and truncation of essentially unlimited frequency spectrum. The discrete set of the time domain voltage values is defined as [40]:

$$U(t) = F \sum_{k=0}^{N} U(k\Delta f) e^{jk\Delta f n \Delta t} \tag{42}$$

where $n = 0, \ldots, N$, F is the highest frequency taken into account, N is the total number of frequency samples, Δf is sampling interval and Δt is the time step.

Finally, the impulse impedance, an also essential parameter in grounding system design, is defined by the following expression [41]:

$$Z_c = \frac{U}{I} \tag{43}$$

where U is the voltage maximum at the discharge point and I is the injected current magnitude at the time instant when U has been reached.

6. Verification of the method

In this part, our model has been verified through comparison with experimental data from other published papers; the validation of our model will also be discussed.

6.1. Verification of the method

To verify the method proposed in this work, some cases solved by other authors are studied.

In the first case, from [42], which gives some grounding impedance measurement results, the grid used for measurement is a 16-mesh grid of 100 m $\times$ 100 m. The earth is modeled by a multilayered earth model. The earth model is given by (a) $\rho_1 = 25\Omega$ m, $\rho_2 = 120\Omega$ m, and thickness of the upper earth is 5 m; (b) $\rho_1 = 120\Omega$ m, $\rho_2 = 25\Omega$ m, $\rho_3 = 250\Omega$ m, thickness of the first and second layers of earth are 5 m and 9 m, respectively. The radius of the grid conductors is 0.5 cm, and they are buried at 0.5 m depth in the earth. Here, the conductivity of the copper conductors is $\sigma_{Cu} = 5.8 \times 10^7$ S/m, and the permittivity of earth is set to $\varepsilon_1 = 5$. The results can be seen in Table 1.

In the second case, which is from [41], a typical grounding grid configuration can be seen in Fig. 2, which was made of round copper conductors with 50 mm^2 cross section. The grounding grid was buried at 0.5 m depth in two-layer horizontal earth, whose resistivity

http://dx.doi.org/10.5772/57049

Earth model	Mea.[42]	Our model
a	0.390	$(0.387, 8.6 \times 10^{-3})$
b	0.658	$(0.652, 1.6 \times 10^{-2})$

Table 1. Comparison with published measurement result: Frequency is 80Hz

ratio for the upper and the lower soil layers is $\rho_1/\rho_2 = 50/20$, the upper layer thickness being $H = 0.6$ m. The inject lightning current parameter was set to $T_1 = 3.5\mu$ s, $T_2 = 73\mu$ s and $I_m = 12.1$ A, the feed point is at the corner of the grid. For our model, the permittivities of the two layer earth model were set to $\varepsilon_1 = 30\varepsilon_0$ and $\varepsilon_2 = 20\varepsilon_0$. The transient SEP can be seen in Fig. 3, which ultimately agreed with the measured curve in Fig. 4 (a) in [41]; meanwhile, the impulse grounding impedance was 2.12 Ω as given by [41], and it is 2.08Ω for our model.

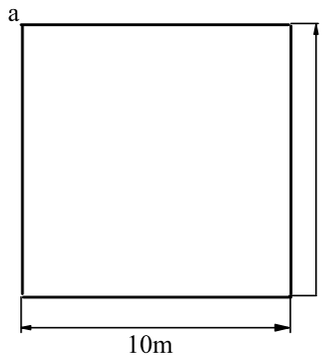

Figure 2. Typical grounding grid configuration

6.2. Validation of our method

The maximum frequency of applicability of the method is limited by the quasi-stationary approximation of the electromagnetic fields, which means the propagation effect of the electromagnetic field around the grounding system can be neglected, so

$$e^{-\gamma_e R} \approx 0 \tag{44}$$

where $\gamma_e^2 = j\omega\mu\left(j\omega\varepsilon_e + \sigma_e\right), e = 1, \ldots, N_e$.

For most of the usual electrodes, this may be applied up to some hundreds of kHz.

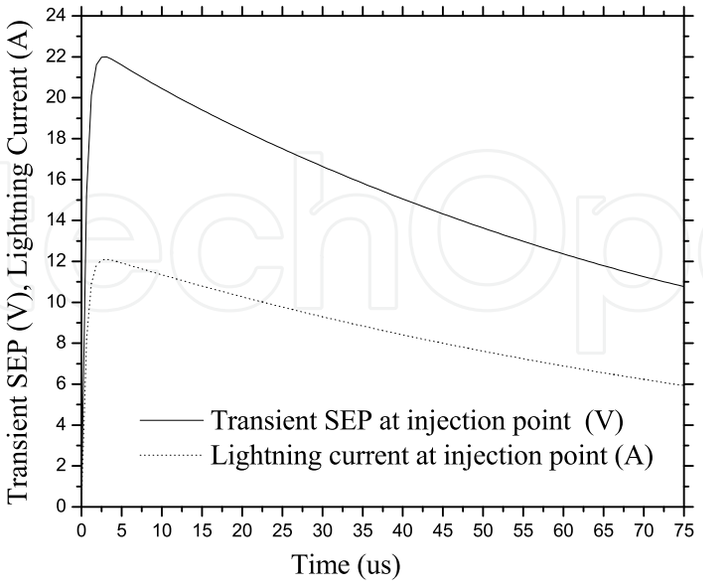

Figure 3. Transient SEP at injection point

7. Simulation result and analysis

A typical grounding system can be seen in Fig. 4. The earth is medalled by a two-layer conductive earth model, whose conductivity and permittivity is $\sigma_1 = 500^{-1}S/m$, $\sigma_2 = 900^{-1}S/m$, $\varepsilon_1 = 10\varepsilon_0$, $\varepsilon_2 = 22\varepsilon_0$, respectively, the first layer height is 5 m. The material of the grounding system conductor is Cu with conductivity $\sigma_{Cu} = 5.8 \times 10^7 S/m$. The conductor radii are 7 mm. The external excited lightning current is injected from the corner of the grounding system, which is described by a double-exponential function: $I(t) = 1.29 \times (e^{-0.019010t} - e^{-0.292288t})$ kA, which means that the parameters of the lightning current are $T_1 = 10\mu$ s, $T_2 = 50\mu$ s and $I_m = 1.29$ kA, the lightning current has been shown in Fig. 5.

The calculated grounding impulse impedance is $(14.401, j1.273)\Omega$.

A comparison between chosen total leakage currents and injecting currents of the grounding system in frequency domain is given in Table 2. It can be seen that the total leakage current of the grounding system is close to the external injected current. All this shows the accuracy of this model.

Freq. (kHz)	injecting currents (kA)	Total leakage currents (kA)
16.7	$(-4.077, -10.964)$	$(-4.078, -10.959)$
125.0	$(-0.486, +0.363)$	$(-0.486, +0.363)$
250.0	$(-0.289, +0.143)$	$(-0.289, +0.143)$
500.0	$(-0.267, -0.070)$	$(-0.267, -0.070)$
800.0	$(-4.301, +3.428)$	$(-4.301, +3.428)$

Table 2. Total leakage currents from the grounding grid and injecting currents in frequency domain

The quasi-static complex image in this case has two terms, the α_n and β_n can be seen below Table 3.

	α_n	β_n
1	$(0.294, -62.137)$	$(9.937, -0.959)$
2	$(0.086, +53.354)$	$(22.453, -11.859)$

Table 3. Quasi-static complex image coefficients

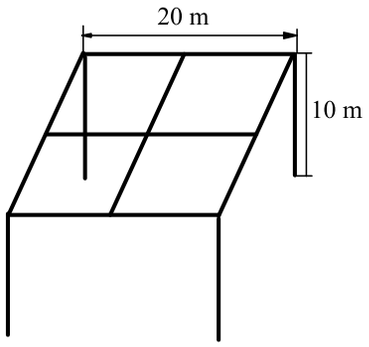

Figure 4. Typical grounding system

The transient SEP at the injection point is given in Fig. 5. From this figure, we can see that the maximum value of the transient SEP at the injection point disagrees with that of the lightning current, the maximum value of the transient SEP at injection point occurs at 12μ s, and the maximum value of the lightning current occurs at 10μ s.

The distribution of absolute values of grounding impedance dependance $|Z(j\omega)|$ on frequency can be seen in Fig. 6. This figure shows that $|Z(j\omega)|$ is independent of the frequency below 100 kHz and equal to the low frequency grounding impedance, which agrees with the viewpoint of [43].

To further discuss the electromagnetic field characteristics along the surface above the grounding grid, the distribution of the electromagnetic field along the surface with three different chosen frequencies (17 kHz, 250 kHz and 800 kHz) have been given in Figs. 7–15. Among these, Figs. 7–9 show the distribution of SEP φ along the surface, Figs. 10–12 show the distribution of the x-component of the EFI, E_x, along the surface, and Figs. 13–15 show the distribution of the x-component of the MFI, B_x, along the surface.

From Figs. 7–9, we know that the ground SEP rise is dependent on the magnitude of the injecting current, the ground SEP rise at 17 kHz is generated by injecting current with (-4.077,-10.964) kA, the ground SEP rise at 250 kHz is generated by injecting current with (-0.289,+ 0.143) kA, and the ground SEP rise at 800 kHz is generated by injecting current

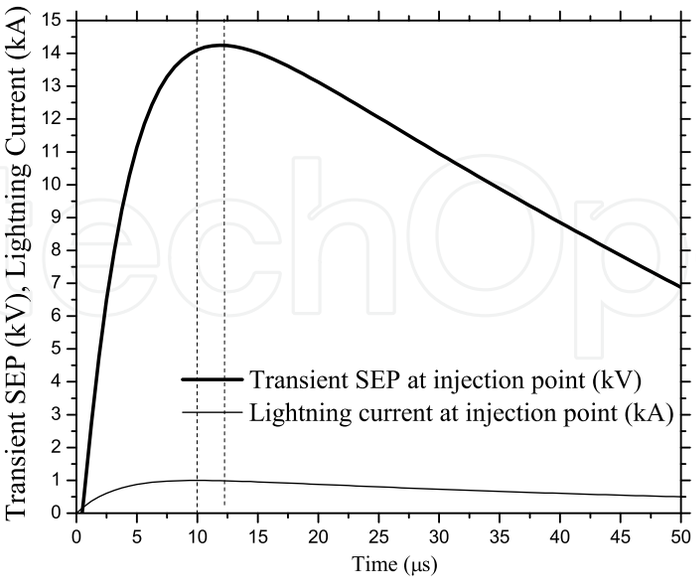

Figure 5. Lightning current

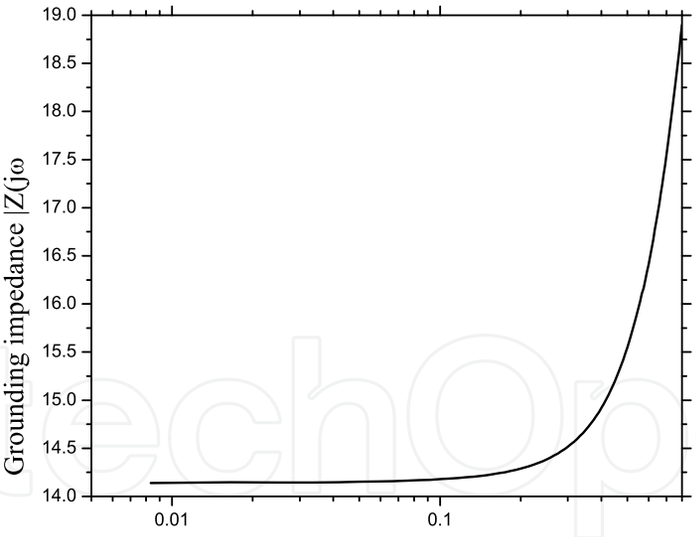

Figure 6. Lightning current

with (-4.301,+ 3.428) kA. So the ground SEP rise at 17 kHz is the maximum, and the ground SEP rise at 250 kHz is the minimum. Meanwhile, we can see that almost an equipotential surface occurs for the low frequency case (17 kHz and 250 kHz), and at higher frequencies, the impedances of the grid conductors are no longer negligible and most of the earth currents dissipate close to the injection point. This phenomenon is well illustrated in Fig. 9 which

http://dx.doi.org/10.5772/57049

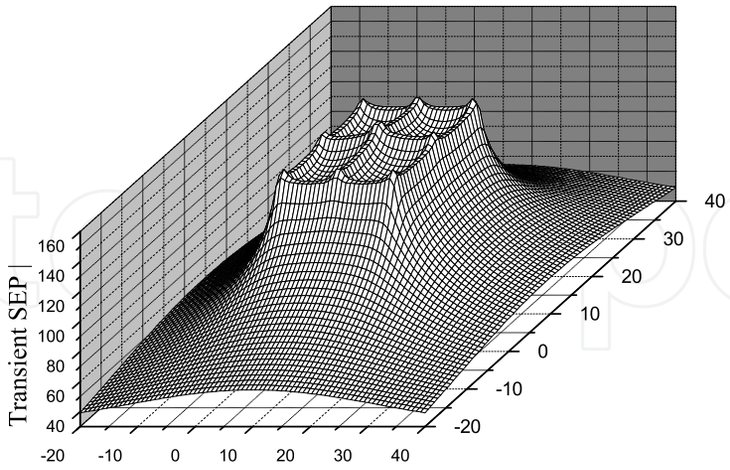

Figure 7. The distribution of the SEP φ on the ground surface (f=16.7 kHz)

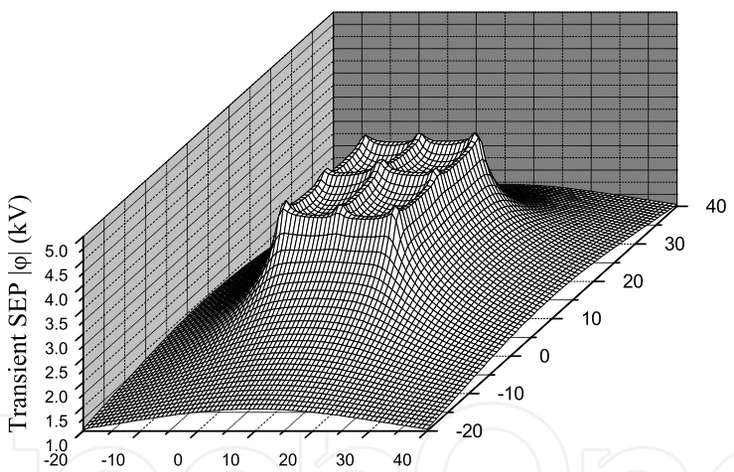

Figure 8. The distribution of the SEP φ on the ground surface (f=250 kHz)

represents the case of a corner current injection. Earth potentials near the injection corner present a very sharp peak, while they are quite low and flat everywhere else, with a minimum at the opposite corner.

From Figs. 10–12, we can see that as in the ground SEP rise case, the maximum value of the x-componential of the EFI E_x is dependent on the magnitude of the injecting current. The distribution of the x-componential of the EFI E_x is along the x-direction. Meanwhile, the distribution of the electrical field is not dependent on the current injection location at low frequencies. This conclusion no longer holds at higher frequencies, as shown in Fig. 12,

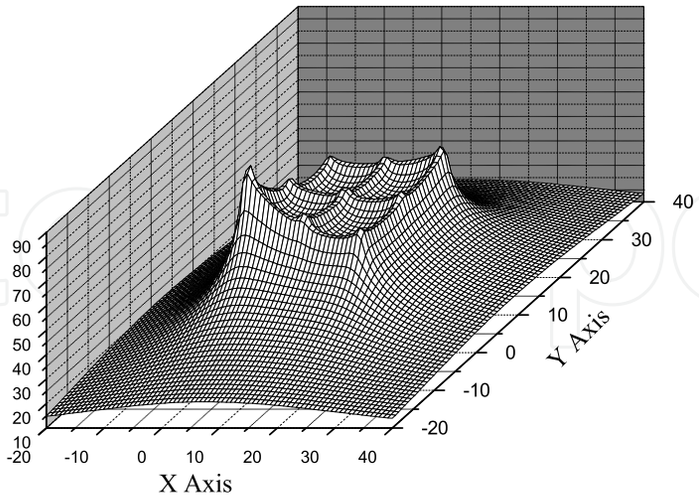

Figure 9. The distribution of the SEP φ on the ground surface (f=800 kHz)

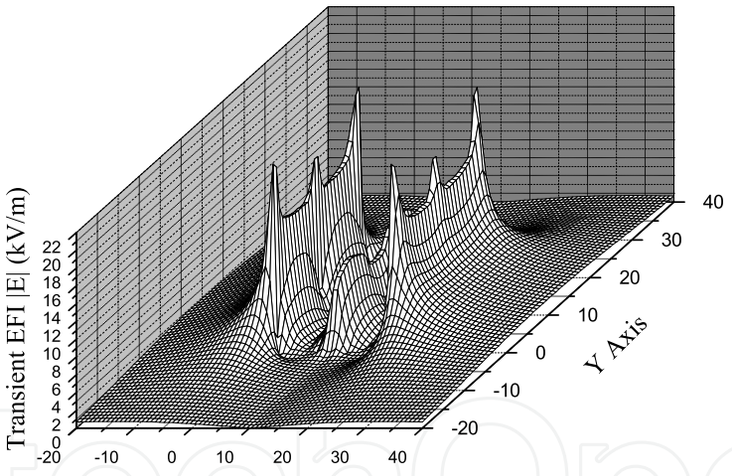

Figure 10. The distribution of the EFI E_x on the ground surface (f=16.7 kHz)

which clearly shows that the region of maximum electrical field shifts from the edge of the grid to the injection point location as the frequency increases from low to high.

The distribution of the x-componential of MFI B_x is given in Figs. 13–15. We can also see that as in the ground SEP rise case, the maximum value of the x-componential of the MFI B_x is dependent on the magnitude of the injecting current. Unlike the distribution of the x-componential of the EFI E_x, the distribution of the x-componential of the MFI B_x is along the y-direction, which can be easily explained in that the distribution of the electrical field is perpendicular to that of the magnetic field. Meanwhile, the distribution of the electrical

http://dx.doi.org/10.5772/57049

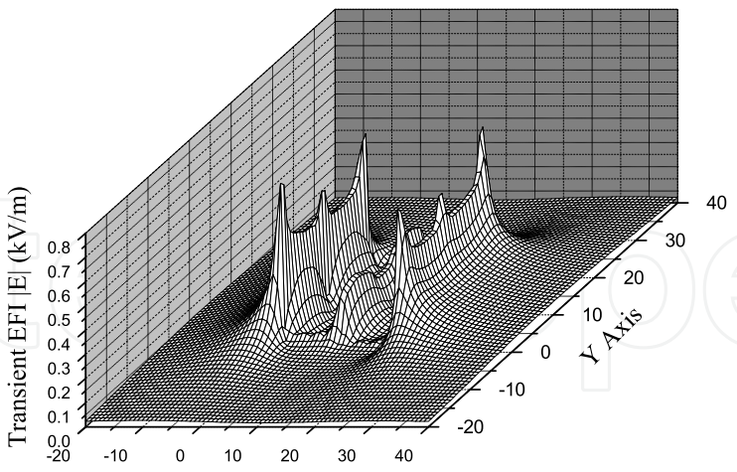

Figure 11. The distribution of the EFI E_x on the ground surface (f=250 kHz)

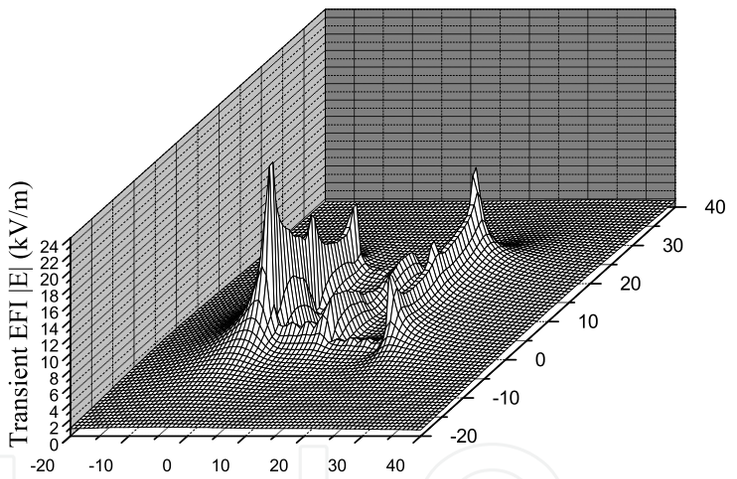

Figure 12. The distribution of the EFI E_x on the ground surface (f=800 kHz)

field is dependent on the current injection location from low to higher frequencies, which is different from the electrical field case.

8. Conclusion

A novel mathematical model for accurately computing the lightning currents flowing in the grounding system of a high voltage a.c. substation, buried in multilayered earth, has been developed in this paper. Together with the FFT, not only the conducting effect of harmonic wave components of these currents, but also capacitive and inductive effects from the interface between different soil layers have been analyzed in the frequency domain. To

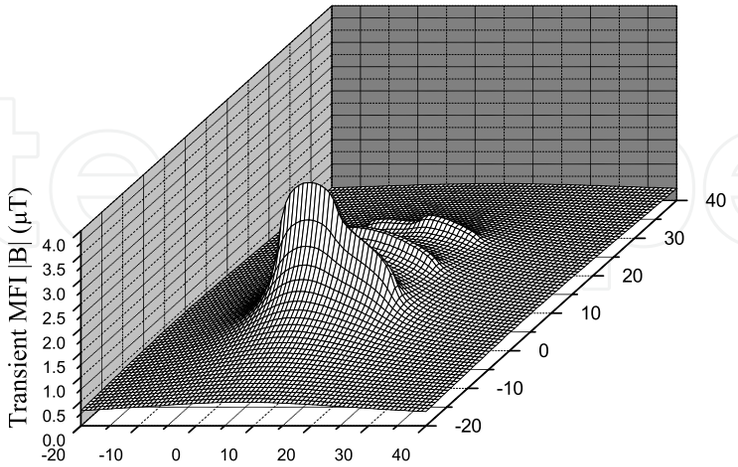

Figure 13. The distribution of the MFI B_x on the ground surface (f=16.7 kHz)

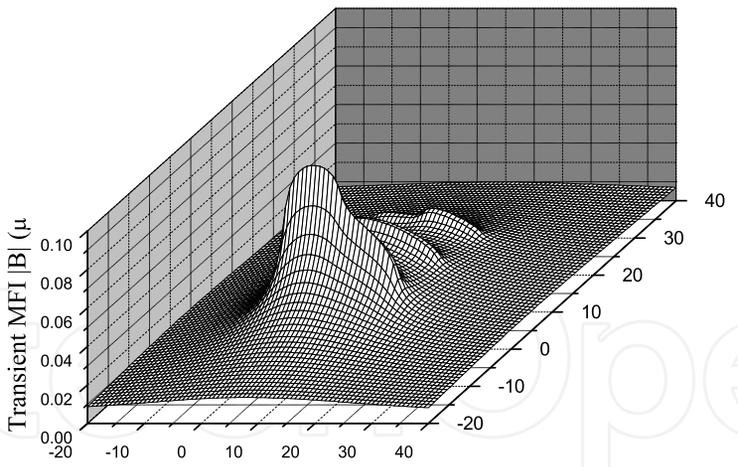

Figure 14. The distribution of the MFI B_x on the ground surface (f=250 kHz)

accelerate the calculation, the QSCIM and a closed form of Green's function were introduced. With the inverse FFT, the model can calculate the distribution of lightning currents in any configuration of the grounding system. This can be used for studying the performance of transient lightning responses to grounding systems. Last, the model has been validated through some numerically simulated and experimental results from open published paper, and some numerical results have been discussed in this paper.

http://dx.doi.org/10.5772/57049

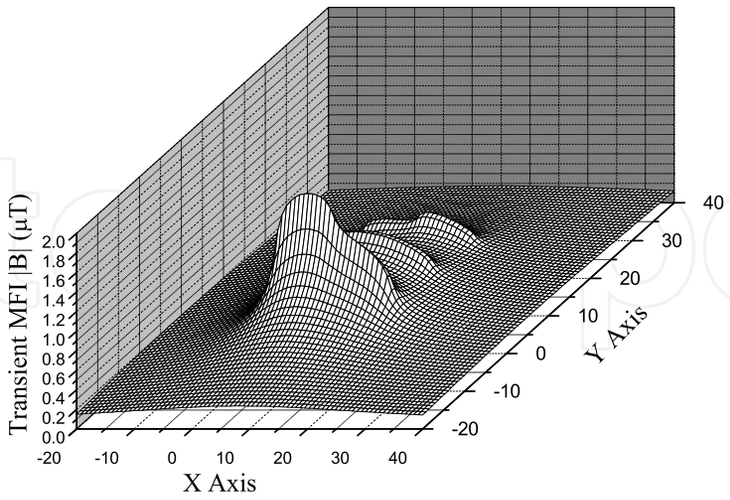

Figure 15. The distribution of the MFI B_x on the ground surface (f=800 kHz)

Acknowledgment

This work was funded by the Science and Technology Projects of State Grid Corporation of China under Contract Number: GY172011000JD and the National Natural Science Foundation of China under Grant 51177153.

Author details

Zhong-Xin Li, Ke-Li Gao, Yu Yin, Cui-Xia Zhang and Dong Ge

China Electrical Power Research Institute, Beijing, China

References

[1] E. D. Sunde. *Earth Conduction Effects in Transmission Systems*, New York: Dover, 1968.

[2] L. V. Bewley, *Traveling Waves on Transmission Systems*, 2nd ed. New York: Wiley, 1951

[3] R. Rudenberg, *Electrical ShockWaves in Power Systems*. Harvard Univ. Press, 1968.

[4] A. P. Meliopoulos, *Power System Grounding and Transients*. New York: Marcel-Dekker, 1988.

[5] A. C. Liew and M. Darveniza, "Dynamic model of impulse characteristics of concentrated earths", *Proc. Inst. Elect. Eng.*, vol. 121, pp. 123–135, Feb. 1974.

[6] J. Wang, A. C. Liew, and M. Darveniza, "Extension of dynamic model of impulse behavior of concentrated grounds at high currents", *IEEE Transactions on Power Delivery*, vol. 20, no. 3, pp. 2160–2165, Jul. 2005.

[7] M. Ramamoorty, M. M. B. Narayanan, S. Parameswaran, and D. Mukhedkar, "Transient performance of grounding grids", *IEEE Transactions on Power Delivery*, vol. 4, no. 4, pp. 2053–2059, Oct. 1989.

[8] A. Geri, "Behaviour of grounding systems excited by high impulse currents: The model and its validation", *IEEE Transactions on Power Delivery*, vol. 14, no. 3, pp. 1008–1017, Jul. 1999.

[9] S. S. Devgan and E. R. Whitehead, "Analytical models for distributed grounding systems", *IEEE Transactions on Power Apparatus and Systems*, vol. PAS-92, no. 5, pp. 1763–1770, Sep./Oct. 1973.

[10] R. Verma and D. Mukhedkar, "Impulse impedance of buried ground wire", *IEEE Transactions on Power Apparatus and Systems*, vol. PAS-99, no. 5, pp. 2003–2007, Sep./Oct. 1980.

[11] C. Mazzetti and G. M. Veca, "Impulse behavior of grounded electrodes", *IEEE Transactions on Power Apparatus and Systems*, vol. PAS-102, no. 9, pp. 3148–3156, Sep. 1983.

[12] R. Velazquez and D. Mukhedkar, "Analytical modeling of grounding electrodes", *IEEE Transactions on Power Apparatus and Systems*, vol. PAS-103, no. 6, pp. 1314–1322, Jun. 1984.

[13] F. Menter and L. Grcev, "EMTP-based model for grounding system analysis", *IEEE Transactions on Power Delivery*, vol. 9, no. 4, pp. 1838–1849, Oct. 1994.

[14] Y. Liu, M. Zitnik, and R. Thottappillil, "An improved transmission-line model of grounding system", *IEEE Transactions on Electromagnetcs Compatibility*, vol. 43, no. 3, pp. 348–355, Aug. 2001.

[15] Y. Liu, N. Theethayi, and R. Thottappillil, "An engineering model for transient analysis of grounding system under lightning strikes: Nonuniform transmission-line approach", *IEEE Transactions on Power Delivery*, vol. 20, no. 2, pp. 722–730, Apr. 2005.

[16] D. Roubertou, J. Fontaine, J. P. Plumey, and A. Zeddam, "Harmonic input impedance of earth connections", in *Proc. IEEE Int. Symp. Electromagnetic Compatibility*, 1984, pp. 717–720.

[17] F. Dawalibi and A. Selby, "Electromagnetic fields of energized conductors", *IEEE Transactions on Power Delivery*, vol. PWRD-8, no. 3, pp. 1275–1284, July 1986.

[18] L. Grcev and Z. Haznadar, "A novel technique of numerical modelling of impulse current distribution in grounding systems", in *Proc. Int. Conf. on Lightning Protection*, Graz, Austria, 1988, pp. 165–169.

[19] L. Grcev and F. Dawalibi, "An electromagnetic model for transients in grounding systems", *IEEE Transactions on Power Delivery*, vol. 5, no. 4, pp. 1773–1781, Oct. 1990.

[20] L. Grcev, "Computation of transient voltages near complex grounding systems caused by lightning currents", in *Proc. IEEE Int. Symp. Electromagnetic Compatibility*, 1992, pp. 393–400.

[21] L. Grcev, "Computer analysis of transient voltages in large grounding systems", *IEEE Transactions on Power Delivery*, vol. 11, no. 2, pp. 815–823, Apr. 1996.

[22] R. Olsen and M. C. Willis, "A comparison of exact and quasi-static methods for evaluating grounding systems at high frequencies", *IEEE Transactions on Power Delivery*, vol. 11, no. 3, pp. 1071–1081, Jul. 1996.

[23] L. Grcev and M. Heimbach, "Frequency dependent and transient characteristics of substation grounding system", *IEEE Transactions on Power Delivery*, vol. 12, no. 1, pp. 172–178, Jan. 1997.

[24] F. Dawalibi, "Electromagnetic fields generated by overhead and buried short conductors, part II—ground networks", *IEEE Transactions on Power Delivery*, vol. PWRD-1, no. 4, pp. 112–119, Oct. 1986.

[25] F. Dawalibi, R. D. Southy, "Analysis of electrical interference from power lines to gas pipelines, Part I, computation methods", *IEEE Transactions on Power Delivery*. vol. PWRD-4. no. 3. pp. 1840–1846, 1989

[26] A. D. Papalexopoulos and A. P. Meliopoulos, "Frequency dependent characteristics of grounding systems", *IEEE Transactions on Power Delivery*, vol. PWRD-2, no. 4, pp. 1073–1081, Oct. 1987.

[27] L. Huang and D. Kasten. "Model of ground grid and metallic conductor currents in high voltage a.c. substations for the computation of electromagnetic fields", *Electric Power Systems Research*. vol. 59. pp. 31–37. 2001.

[28] A. F. Otero, J. Cidras, and J. L. Alamo. "Frequency-dependent grounding system calculation by means of a conventional nodal analysis technology", *IEEE Transactions on Power Delivery*, vol. PWRD-14, no. 3, pp. 873–877, July 1999.

[29] Z. X. Li, W. J. Chen, J. B. Fan and J. Y. Lu. "A novel mathematical modeling of grounding system buried in multilayer earth", *IEEE Transactions on Power Delivery*. vol. PWRD-21, no. 3, pp. 1267–1272. 2006.

[30] Z. X. Li and W. J. Chen, "Numerical simulation grounding system buried within horizontal multilayer earth in frequency domain", *Communications in Numerical Methods in Engineering*. vol. 23, no. 1, pp. 11–27. 2007.

[31] Z. X. Li and J. B. Fan. "Numerical Calculation of Grounding System in Low Frequency Domain Based on the Boundary Element Method", *International journal for numerical methods in engineering*, vol. 73, pp. 685–705, 2008.

[32] Z. X. Li, G. F. Li, J. B. Fan, and C. X. Zhang. "Numerical calculation of grounding system buried in vertical earth model in low frequency domain based on the boundary element method", *European Transactions on Electrical Power*, vol. 19, no. 8, pp. 1177–1190. 2009

[33] J. R. Wait and K. P. Spies, "On the representation of the quasi-static fields of a line current source above the ground", *Canadian Journal of Physics*, vol. 47, pp. 2731–2733. 1969.

[34] D. J. Thomson, J. T. Weaver et al., "The complex image approximation for induction in a multilayer earth", *Journal of Geophysical Research*, vol. 80, pp. 123–129. 1975.

[35] J. Choma. *Electrical Networks—Theory and Analysis*, New York, 1985

[36] R. J. Heppe. "Computation of potential at surface above an energized grid or other electrode, allowing for non-uniform current distribution", *IEEE Transactions on Power Apparatus and Systems*. vol. PAS-98, no. 6, pp. 1978–1989. 1979

[37] R. S. Adve, T. K. Sarkar. 'Extrapolation of time-domain responses from three-dimensional conducting objects utilizing the Matrix Pencil technique', *IEEE Transactions on Antenna and Propagation*. Vol. AP-45, no. 1, pp: 147-156. 1997.

[38] P. L. Zhang, J. S. Yuan and Z. X. Li, "The complex image method and its application in numerical simulation of substation grounding grids", *Communications in Numerical Methods in Engineering*. vol. 15, no. 11, pp. 835–839. 1999.

[39] I. S. Gradshteyn and I. M. Ryzhik, *Tableof integrals, Series and Products*, Correction and enlarged edition, ACADEMIC PRESS, a Subsidiary of Harcourt Brace Jovanovich Publishers. NewYork, London, Toronto Sydney, San Francisco.

[40] R. E. Ziemer and W. H. Tranter, Principles of Communications, Houghton Mifflin Company, Boston, 1995.

[41] Z. Stojkovic, J. M. Nahman, D. Salamon, and B. Bukorovic, "Sensitivity analysis of experimentally determined grounding grid impulse characteristic", *IEEE Transactions on Power Delivery*, vol. 13, no. 4, pp. 1136–1143, Oct. 1998.

[42] J. X. Ma and F. P. Dawalibi. "Influence of inductive coupling between leads on ground impedance measurements using the fall-of-potential method", *IEEE Transactions on Power Delivery*. vol. 16, no. 4, pp. 739–743. Oct., 2001.

[43] L. Grcev, "Impulse efficiency of ground electrodes", *IEEE Transactions on Power Delivery*, vol. PWRD-24, no. 1, pp. 441–452, Jan. 2009.